(1) pathogenic,
(2) likely pathogenic,
(3) uncertain significance,
(4) likely benign,
(5) benign

・Variant の記載は，A standard gene variant nomenclature <http://www.hgvs.org/mutnomen> に従う．臨床における報告書には，DNA レベルのバリアントの記載として下記を含めて記載する
(e.g., “g.” for genomic sequence, “c.” for coding DNA sequence, “p.” for protein, “m.” for mitochondria, etc)

・Variant の評価は，種々のデータベース，および In sillico predictive program 等を用いて行う．
データベースについては，以下を確認する．
1) データベースのアップデート，データキュレーションの方法，
2) バリアントの HGVS 命名， genome build, transcript references,
3) 分析における正確性（NGS の deapth とサンガー法での確認，etc），
4) データソースと独立性

・結果報告書には，CLIA 規制，ACMG，CAP の NGS Checklist guidelines にしたがって，Results, Interpretation, References, Methodology, appropriate disclaimers を記載する．

・ナンセンス，フレームシフト，スプライスサイトの変異，エクソンレベルの欠失など，遺伝子，あるいはそれに由来するタンパクに有害なものだったとしても，病気の原因であると断定するには不十分であり，de novo 変異が直ちに病的変異であることを意味しないことには注意すべきである．現状ではバリアントの情報は不完全であり，100%正しいということを意味していない．可能な限り，他の臨床情報と合わせて，総合的に判断するべきである．

2）症例集積

H26 年度は 1 月末現在，36 家系 39 例の原因不明の MCA/ID 症例と症例の親 41 名，さらに G 分染法により構造異常が指摘された 2 症例および MLPA 法で部分欠失が指摘された 1 症例を収集し，36 家系までマイクロアレイ染色体解析を実施した．

原因不明の患者では 8 例（20%）に各症例の疾患と関連している可能性の高いゲノムコピー数異常（pathogenic and likely pathogenic CNVs: pCNVs）を検出した．

原因不明の異なる症状の先天異常を有する姉妹に検出された 1q21.1-q21.2 の約 1.2Mb のゲノムコピー数減少は，International Collaboration for Clinical Genomics（ICCG）が運営している ISCA Database に “1q21.1 microdeletion” として “Curated Pathogenic” と評価されている 9 個の OMIM genes を含む領域と近似の CNV であり，35 万種類以上の bCNVs を登録している Database of Genomic Variants（DGV）にもこの領域全体にわたる登録はなかったことから，当初 pCNV と考えた．しかしながら，確認のため実施した両親の解析で特に症状を有しない母親に同じ CNV が検出された．

1 例に OMIM genes と RefSeq gene を各 1 個含む 2p14 に約 680kb のコピー数減少を検出した．DGC に全領域にわたる登録はないため，症状に関連する可能性を考えたが，特に症状を有しない父親に同じ CNV を認めた．

1 症例に認めた約 1.5Mb の 2q12.2-2q12.3 のゲノムコピー数減少は，3 個の OMIM genes を含む領域と近似の CNV であり，イギリスのサンガー研究所が運営する DECIPHER (DatabasE of Genomic variants and Phenotype in Humans Using Ensembl Resources)に近似症例が複数登録されていたこと，DGV に全領域にわたる登録がなかったことから pCNV を疑った．しかし，特に症状を有しない母親に同じ CNV を検出した．

1 症例に 1 個の OMIM gene を含む約 750kb の 6q16.1 のゲノムコピー数減少を検出した．DGV に全領域にわたる登録はなく，DECIPHER でもより小さい範囲に 1 例登録があったため，症状に関連する可能性を考えたが，特に症状を有しない母親に同様の CNV を認めた．

1症例に7q端部重複と18p端部欠失を認めた．本人および両親のFISH解析により，片親が均衡型転座保因者であることが確認された．

1症例にISCA Databaseに“9q subtelomeric deletion”としてCurated Pathogenicと評価されている領域内の1個のOMIM genesを含む領域と近似の約470kbのコピー数減少を検出した．FISH解析で検証し，9q34欠失症候群と診断した．

責任遺伝子の*FGFR3*にcommonなmutationが検出されなかった知的障害を伴う軟骨無形成症患者に実施したマイクロアレイ解析で22q11.21に2.5Mbのコピー数増加を認めた．ISCA Databaseでも“Common Larger 22q11 duplication”として“Curated Pathogenic”として登録されている，欠失変異もある約2.8Mbの領域であった．しかし，特に症状を有しない母親に同じCNVを検出した．

微細染色体構造異常が判明していた3症例は，いずれも臨床的に有用な詳細が判明した．

検査センターにより実施されたG分染法で3q25-q26.3の欠失と報告されていた症例は，臨床遺伝専門医の臨床的再評価により blepharophimosis, ptosis, and epicanthus inversus 症候群（BPES）であると診断されたが，染色体検査結果は3q22.3に座位するBPESの責任遺伝子*FOXL 2*を含んでおらず，バンドの判定が不正確であることが示唆された．マイクロアレイ解析および検証のFISH解析を実施し，症例は*FOXL 2*を含む3q22.1-q24の16.3Mbの欠失であることを確認した．

2q端部の欠失あるいは由来不明の不均衡型構造異常と報告されていた症例は，2q端部以外にコピー数異常は認めなかったため，おそらく2qの端部欠失であることとその大きさが約9.5Mbであることが確認された．

高CK血症よりジストロフィン異常症を疑われ検査センターにて実施されたMLPA法による*DMD*遺伝子のコピー数解析で部分欠失を指摘されたが，症状からDMD以外の遺伝子におよぶ欠失を疑われマイクロアレイ解析が実施された．MLPA法による*DMD*遺伝子の欠失領域が検証されるとともにさらにセントロメア寄りに約1.7Mb計3.4Mbにおよぶ欠失であることがマイクロアレイ解析および検証のFISH解析により確認された．

D．考察

genome-scale sequencing（WGS/WES）は当初，すぐに医療に役立つと考えられていたが，臨床応用に用いる場合には大きなバリアがあることが分かってきた．臨床的に有用なバリアントを評価するためには多くの時間とエフォートが必要であり，複雑な結果をどのように患者に伝えるのかは大きな問題である．従来の伝統的な遺伝学的検査の場合とは異なる方法が求められる．

ACMGでは，2013年にIFに関するステートメントを公表したが，その後も活発な議論が行われ，2014年に新たなステートメントを公開した．開示すべき56の遺伝子リストに変更はないが，偶発的所見（IF, incidental findings）ではなく，積極的に検出すべき二次的所見（SF, secondary findings）と用語が代わり，インフォームド・コンセントの重要性が改めて強調されている．

ここで注意しなければならないのは，ACMGステートメントは，臨床の場で診療目的にgenome-scale sequencing（WGS/WES）を行う場合には，治療法・予防法が存在し，医学的に有用と考えられる疾患（現在は56疾患）の遺伝子については解析を行うべきであることを前提に，当初の目的とは異なる病気の遺伝子の変化がわかった場合の開示方法，および検査前のインフォームド・コンセントのあり方が記載されていることである．決して，予期しない変異がたまたま見つかったときにどうするかについての議論ではないことに留意すべきである．

わが国では，エクソーム解析をはじめとするgenome-scale sequencingのほとんどが研究目的で行われており，ACMGステートメントをそのまま運用することはできない．しかし，研究目的ではあっても，これを行う場合には，常に偶発的所見が得られる可能性があり，ACMGステートメントを初めとする国際的な議論を注視しておかなければならない．

現在，ACMGで作成準備が進められている塩基配列多様体（シークエンス・バリアント）の解釈に関す

る標準ガイドラインにも注視しておく必要がある．今後，genome-scale sequencing により生み出される膨大なバリアントの解釈を進めなければならないが，そのためにはデータベース，とくに日本人のゲノムデータベースを構築しておかなければならない．

バリアントの情報（ゲノム情報）は，あるかないかのデジタルな情報であるが，それがどのような意味をもつのかを判断するために必要となるデータベースは不完全であり，臨床の場で用いる際には，ゲノム情報だけではなく，他のさまざまな情報と合わせて総合的に判断すべきである．

原因不明の先天異常症例において，マイクロアレイ染色体解析で診断が確定した症例以外は，主治医による臨床症状の再評価を実施し，網羅的エクソーム解析の候補症例として数例を絞り込んだ．

原因不明の患者のうち6家系にpCNVsと考えられるゲノムコピー数異常を6領域に検出した．うち5領域は特に症状を伴わない親に同じCNVsが確認された．数万例の解析結果を登録した海外のデータベースで“Curated Pathogenic”と評価している領域も含まれていた．

すでに300万サンプル以上，35万種類以上のbCNVsを登録しているDGVにも登録されていないCNVsが検出されるということは，ごく稀なゲノムバリアントはまだまだ存在することが示唆された．また，2005年にBarberが，特に症状を伴っていない染色体不均衡型構造異常例をreviewした論文（J Med Genet, 2005）を発表し，“The Chromosome Anomaly Collection”としてデータベース化している．これらはマイクロアレイ解析が開発される以前の症例が多いため異常領域は正確でないが，10Mbを超えると推定される大きなサイズの異常を有する症例も含まれている．こういったサイズでもbenignとなる領域がヒトゲノムにはあるということを，我々はこのような症例から学ばなくてはならない．

また，ICCGで評価されたCNVsでも特に同様の症状を有しない親由来が判明する場合もあり，一旦評価が決まったバリアントであっても今後評価が変わる可能性もあることが本解析結果からも示された．その理由としては，症状や病態と関連はあるが浸透率が低いものである可能性，別の領域の修飾因子が関係している可能性などが考えられるが，この事実はマイクロアレイ染色体検査を臨床検査として実施する際に十分留意する必要がある．

軟骨無形成症患者に“Common Larger 22q11 duplication”のCNVが検出されたが，これは伴っているIDの原因である可能性があるものの，親由来が確認されたため評価に苦慮している．一方でこの結果は，ひとりの患者が複数の先天異常の原因を有することも考慮する必要があることを示している．a

現在，わが国では原因不明の先天異常患者の診断目的に実施する遺伝学的検査は，保険で実施可能なG分染法が最初で，異常がなければ研究としてマイクロアレイ染色体検査，それに異常がなければ研究としてWESという流れである．しかしながら，国際的には臨床検査としてマイクロアレイ染色体検査を最初に実施する流れである．さらにNGS解析による症例あたりのコストが下がってきている現状で，昨年度あたりから一部の国際的にゲノム解析をリードしている施設ではWESを最初に実施する傾向すらみえてきた．

マイクロアレイ染色体検査を実施した患者のほとんどがG分染法を実施していること，本研究で解析した微細染色体構造異常が判明していた3症例のいずれも臨床的に有用な情報が追加されたことからも，原因不明の先天異常症例に最初に実施すべき遺伝学的検査をやはりG分染法よりマイクロアレイ染色体検査とすることが，さらに費用さえ確保できるのであればWESを最初に実施することが，診断をつけるために最も効率がよいことは明らかである．医療制度の異なるわが国においても，せめて国際標準にこれ以上の遅れをとらないようマイクロアレイ染色体検査を臨床検査として実施できる体制整備が急務である．ゲノムバリアントの結果解釈が単純でないことはマイクロアレイ染色体検査に限らず，WESにおいてもWGSにおいても，サンガーシーケンス解析においても同様のはずである．NGSによりCNVsを検出するソフトの開発が進んでいるが，そのアルゴリズムの改良のためにもどのようなCNVsが検出されるかを把握しておくことは必要である．染色体不均衡

型構造異常も CNVs も含む多数の正常日本人ゲノムバリアントのデータベース整備が必要である．

一方，ゲノムバリアントに伴う染色体再構成はFISH解析による染色体分裂像の解析が必須で，特に不均衡型染色体構造異常が疑われるパターンのCNVsが検出された場合，両親の染色体分裂像を用いた均衡型構造異常を検出するための FISH 解析が重要である．さらにマイクロアレイでは検出できない（プローブが配置できない）複数の染色体と共通するシーケンスを有する末端部や端部着糸点型染色体短腕などもゲノムの一部であることを再認識する必要がある．マイクロアレイ染色体検査で端部欠失のパターンであっても実は不均衡型構造異常である場合があることを我々は経験している．染色体核型分析技術の継承，担当者の人材育成も必要である．

E．結論

パーソナルゲノム時代における網羅的エクソーム解析の倫理的課題について検討した．個人ゲノム情報を適切に医療の場に反映させる医療提供体制のあり方についての提言をめざしてさらに情報収集を継続する．網羅的エクソーム解析の対象となる症例のさらなる集積に努める．

F．健康危険情報

特になし

G．研究発表

1．論文発表

Wakui K. Study of structural chromosome abnormalities to increase the understanding of human genetic diversity: a commentary on signature of backward replication slippage at the copy number variation junction. J Hum Genet. 2014 Nov;59(11):591-2.

Mishra D, Kato T, Inagaki H, Kosho T, Wakui K, Kido Y, Sakazume S, Taniguchi-Ikeda M, Morisada N, Iijima K, Fukushima Y, Emanuel BS, Kurahashi H. Breakpoint analysis of the recurrent constitutional t(8;22)(q24.13;q11.21) translocation. Mol Cytogenet. 2014 Aug 13;7:55

Narumi Y, Nishina S, Tokimitsu M, Aoki Y, Kosaki R, Wakui K, Azuma N, Murata T, Takada F, Fukushima Y, Kosho T. Identification of a novel missense mutation of MAF in a Japanese family with congenital cataract by whole exome sequencing: a clinical report and review of literature. Am J Med Genet A. 2014 May;164A(5):1272-6.

Shimizu K, Wakui K, Kosho T, Okamoto N, Mizuno S, Itomi K, Hattori S, Nishio K, Samura O, Kobayashi Y, Kako Y, Arai T, Tsutomu OI, Kawame H, Narumi Y, Ohashi H, Fukushima Y. Microarray and FISH-based genotype-phenotype analysis of 22 Japanese patients with Wolf-Hirschhorn syndrome. Am J Med Genet A. 2014 Mar;164A(3):597-609.

2．学会発表

西恵理子，涌井敬子，荒川経子，古庄知己，川目裕，福嶋義光．20q11.2 領域の微細欠失を認めた男児例．日本小児遺伝学会学術集会，2014 年 4 月 9-10 日，名古屋 （ポスター発表）

涌井敬子，福嶋義光．B リンパ芽球様細胞株の樹立により生じうるゲノムコピー数異常．日本小児遺伝学会学術集会，2014 年 4 月 9-10 日，名古屋

Nishi E, Wakui K, Arakawa M, Kawame H, Fukushima Y, Kosho T. An interstitial microdeletion of 20q11.21 in a boy with cheilognathopalatoschisis, anorectal malformation, severe microcephaly, craniofacial features, feeding difficulty, mild growth impairment, and mild intellectual disability. The European Human Genetics Conference 2014, 2014 年 5 月 31 日-6 月 3 日，Milano（ポスター発表）

涌井敬子，福嶋義光．各種遺伝学的解析法による染色体異常診断に関する考察．第 38 回日本遺伝カウンセリング学会学術集会．2014 年 6 月 26 日-29 日，東大阪

岸本洋子、荒木尚美、涌井敬子、望月純子、峰尾絵梨、高梨学、福田令、石井正浩、海野信也、福嶋義光、高田史男．15 番染色体長腕端部欠失を持つ左心低形成症候群の双胎 1 児．第 54 回日本先天異常学会学術集会．2014 年 7 月 26 日-27 日，相模原

Takano K, Nishimura T, Wakui K, Takahashi S, Inaba Y, Kosho T, Fukushima Y. A duplication of the *CDKL5* gene identified in a boy with developmental delay with autistic behavior, short stature and microcephaly. American Society of Human Genetics, 2014 年 10 月 18-22 日， San Diego （ポスター発表）

Nishi E, Wakui K, Arakawa M, Hirabayashi S, Fukushima Y, Kosho T. An interstitial microdeletion of 4q21 in a girl with pituitary hypoplasia , epilepsy, severe growth impairment, and profound intellectual disability. American Society of Human Genetics, 2014 年 10 月 18-22 日， San Diego （ポスター発表）

Hatano C, Yokoi T, Wakui K, Enomoto K, Kuroda Y, Ohashi I, Kosaki R, Kurosawa K. Contiguous deletion of CADPS2 and GRM8 associates with severe autism spectrum disorder. American Society of Human Genetics, 2014年10月18-22日, San Diego（ポスター発表）

涌井敬子、山口智美、江口真理子、山内俊史、太田雅明、檜垣高史、石井榮一、福嶋義光. CGH+SNPアレイを用いた特定染色体領域のgenotyping評価の試み：トリソミー14モザイク症例の2細胞系列の14番染色体親由来推定. 日本人類遺伝学会第59回大会, 日本遺伝子診療学会第21回大会. 2014年11月19日-22日, 東京

西恵理子、涌井敬子、荒川経子、平林伸一、福嶋義光、古庄知己. 4q21微細欠失症候群の女児例. 日本人類遺伝学会第59回大会, 日本遺伝子診療学会第21回大会. 2014年11月19日-22日, 東京（ポスター発表）

H. 知的財産権の出願・登録状況

1. 特許取得

なし

2. 実用新案登録

なし

3. その他

なし

研究成果の刊行に関する一覧表

書籍

著者氏名	論文タイトル名	書籍全体の編集者名	書　籍　名	出版社名	出版地	出版年	ページ

雑誌

発表者氏名	論文タイトル名	発表誌名	巻号	ページ	出版年
Miyatake S,*Matsumoto N (*: correspondence).	Clinical exome sequencing in neurology practice.	Nat Rev Neurol	10(12)	676-678, 2	2014
Tsurusaki Y, et al., *Matsumoto N.	De novo SOX11 mutations cause Coffin-Siris syndrome. Nat Commun	Nat Commun	5	4011	2014
Miyatake S, et al., *Matsumoto N, *Saitsu H (*: co-correspondence)	Expanding the phenotypic spectrum of TUBB4A-associated hypomyelinating leukoencephalopathies,	Neurology	82(24)	2230-2237	2014
*Kato M, et al., Matsumoto N.	PIGA mutations cause early-onset epileptic encephalopathies and distinctive features.	Neurology	82(18)	1587-1596,	2014
*Nakamura K, et al., Matsumoto N, Saitsu H.	AKT3 and PIK3R2 mutations in two patients with megalencephaly-related syndromes.	Clin Genet	85(4):	396-398	2014
*Miyake N, et al., Matsumoto N.	Ehlers–Danlos syndrome associated with glycosaminoglycan abnormalities. J. Halper (ed.), Progress in heritable soft connective Tissue diseases,	Advances in Experimental Medicine and Biology	802	145-159	2014

Ohba C, et al., *Matsumoto N, *Saitsu H (*: co-corresponden ce).	PIGN mutations cause congenital anomalies, developmental delay, hypotonia, epilepsy, and progressive cerebellar atrophy.	Neurogenet	59(5)	292-295	2014
Ohba C, et al., *Matsumoto N, *Saitsu H (*: co-corresponden ce).	Early onset epileptic encephalopathy caused by de novo SCN8A mutations.	Epilepsia	55(7)	994-1000	2014
#Miyatake S, #Koshimizu E (# denotes equal contribution), et al., *Matsumoto N.	Deep sequencing detects very low-grade somatic mosaicism in the unaffected mother of siblings with nemaline myopathy.	Neuromuscul Disord	24(7)	642-647	2014
Nakashima M, et al., Matsumoto N*.	Novel compound heterozygous PIGT mutations caused multiple congenital anomalies-hypotonia-s eizures syndrome 3.	Neurogenet	15(3)	193-200	2014
Miyake N (: corresponding author), et al., Matsumoto N.	Numerous BAF complex genes are mutated in Coffin-Siris syndrome.	Am J Med Genet Part C	166(3)	257-261	2014
Katagiri S, et al., Matsumoto N, et al.	Whole exome analysis identifies frequent CNGA1 mutations in Japanese population with autosomal recessive retinitis pigmentosa.	Plos One	9(9)	e108721	2014
Tsurusaki Y, et al., *Matsumoto N	Whole exome sequencing revealed causative biallelic IFT122 mutations in a family with CED1 and recurrent pregnancy loss.	Clin Genet	85(6)	592-594	2014
Tsurusaki Y, et al., *Matsumoto N.	Coffin-Siris syndrome is a SWI/SNF complex disorder.	Clin Genet	85(6)	548-554	2014

Ohashi T, et al., Matsumoto N, et al.	Infantile epileptic encephalopathy with a hyperkinetic movement disorder and hand stereotypies arising from a novel SCN1A mutation.	Epileptic Disord	16(2)	208-212	2014
Wakui K.	Study of structural chromosome abnormalities to increase the understanding of human genetic diversity: a commentary on signature of backward replication slippage at the copy number variation junction.	J Hum Genet.	59(11)	591-592	2014
Mishra D, Kato T, Inagaki H, Kosho T, Wakui K, Kido Y, Sakazume S, Taniguchi-Ikeda M, Morisada N, Iijima K, Fukushima Y, Emanuel BS, Kurahashi H.	Breakpoint analysis of the recurrent constitutional t(8;22)(q24.13;q11.21) translocation.	Mol Cytogenet.	7	55	2014
Narumi Y, Nishina S, Tokimitsu M, Aoki Y, Kosaki R, Wakui K, Azuma N, Murata T, Takada F, Fukushima Y, Kosho T.	Identification of a novel missense mutation of MAF in a Japanese family with congenital cataract by whole exome sequencing: a clinical report and review of literature.	Am J Med Genet A.	164A(5)	1272-1276	2014
Shimizu K, Wakui K, Kosho T, Okamoto N, Mizuno S, Itomi K, Hattori S, Nishio K, Samura O, Kobayashi Y, Kako Y, Arai T, Tsutomu OI, Kawame H, Narumi Y, Ohashi H, Fukushima Y.	Microarray and FISH-based genotype-phenotype analysis of 22 Japanese patients with Wolf-Hirschhorn syndrome	Am J Med Genet A.	164A(3)	597-609	2014

GENETICS

Clinical exome sequencing in neurology practice

Satoko Miyatake and Naomichi Matsumoto

Clinical exome sequencing (CES) is becoming a standard tool for molecular diagnosis of genetic disorders, with a diagnostic yield of approximately 25%. New studies demonstrate the favourable diagnostic yield of CES for both early-onset and adult-onset neurogenetic disorders. These studies demonstrate the strengths, limitations and potential of CES in neurology practice.

Miyatake, S. & Matsumoto, N. *Nat. Rev. Neurol.* **10**, 676–678 (2014); published online 4 November 2014; doi:10.1038/nrneurol.2014.213

Whole-exome sequencing (WES), termed clinical exome sequencing (CES) when used for clinical diagnosis, is currently being integrated into standard medical practice.[1] This new development raises questions regarding the efficiency of CES for the diagnosis of neurogenetic disorders. Two extensive studies on CES, one focusing on cerebellar ataxia[2] and the other on paediatric neurology,[3] have recently addressed this question.

> "...WES can realistically be used for diagnosis of patients with suspected genetic disorders..."

In the first study, Fogel *et al.*[2] described CES in 76 patients (mean age 49 years) with cerebellar ataxia, mainly of the sporadic (56 of 76 patients, 74%) and adult-onset (55 of 76 patients, 72%) type. The authors reported a definitive diagnostic yield of 21%, which compares favourably with other CES studies mainly targeting early-onset diseases. Importantly, common repeat expansion disorders that cause hereditary cerebellar ataxia were excluded in all patients before enrolment. In the second paper, Srivastava *et al.*[3] reported a CES study in 78 paediatric patients (mean age 8.6 ± 5.8 years) with various unexplained neurodevelopmental disorders. The presumptive diagnostic yield was 41% (32 of 78), including patients with pathogenic variants previously reported as disease-associated, and patients with novel, probably pathogenic variants in a disease-associated gene.

These studies clearly indicate that the diagnostic yield of CES for neurogenetic disease is high, and CES is beneficial to neurology practice for diagnosis of both early-onset and adult-onset cases. Although approximately 60–80% of patients would not achieve a definitive molecular diagnosis at present, accumulation and later re-evaluation of CES data for similar diseases might lead to identification of previously unknown causative genetic variations.

Since the introduction of next-generation sequencing (NGS) technology in 2004, researchers have been able to simultaneously investigate the >20,000 genes that comprise the human genome. WES, as opposed to whole-genome sequencing, is used to sequence (almost) all known coding exonic regions, which comprise only 1–2% of the human genome but harbour around 85% of causative mutations for genetic diseases.[4] Since 2010, WES has been successfully applied to Mendelian disorders of unknown genetic aetiology, and has identified numerous mutant genes.[5,6] The power of WES is further demonstrated by the identification of *de novo* and mosaic mutations.[7] The number of phenotypes with a demonstrated molecular basis in the Online Mendelian Inheritance in Man (OMIM) database has grown from 2,048 in January 2007 to 4,247 in October 2014, mostly owing to WES.

The current cost of WES per person might only be twofold to fourfold higher than that of some single-gene Sanger sequencing tests.[1] This rapidly decreasing cost combined with superior efficiency, means that WES can realistically be used for diagnosis of patients with suspected genetic disorders, especially for highly heterogeneous diseases, thereby avoiding the potential 'diagnostic odyssey' of the past. In 2012, the first diagnostic CES study of 100 trios with intellectual disability had a diagnostic yield of 16%.[8] Subsequent CES studies reported a yield of around 25%, depending on the target disease.[6,8,9]

CES studies of cerebellar ataxia such as that of Fogel *et al.*[2] are complicated by the highly heterogeneous nature of the disease, comprising >60 primary neurogenetic conditions and nearly 300 additional genetic conditions. Although the technique cannot reliably detect copy number variants, indels of >10 nucleotides, structural variants, repeat expansion, aneuploidy and epigenetic alterations,[1] the authors were able to identify clinically relevant genetic information in 61% of patients (46 of 76). Overall, these data translated to a diagnosis in 21% of patients (16 of 76), all of whom harboured known disease-causing mutations or mutations causing protein truncation in genes with a previously established disease association. However, 40% of patients (30 of 76) harboured highly suspicious potentially pathogenic—but unproven—variants, warranting further investigation.

Patients with conclusively diagnostic mutations in the study by Fogel *et al.*[2] mostly had sporadic (11 of 16, 69%) and recessive (10 of 11, 91%) mutations, which are typically easier to detect in data from a single

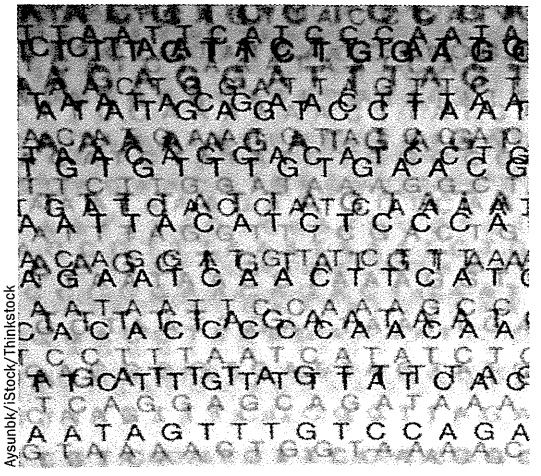

Aysunbk/iStock/Thinkstock

clinical exome sequence than are dominant mutations. Although the diagnostic yield for adult patients (onset age >20 years) was lower than in patients with early-onset disease (11% compared with 48%), of those who were diagnosed, most were sporadic cases (4 of 6, 67%), suggesting that CES can be used to diagnose sporadic cases of cerebellar ataxia. By contrast, a 'presumptive' diagnostic yield of 41%, as reported by Srivastava *et al.*,[3] seems high compared with similar studies investigating intellectual disability (16–31%).[8,9] However, this diagnostic yield includes patients with 'likely pathogenic' variants that might require further investigation.

> "...CES is beneficial to neurology practice for diagnosis of both early-onset and adult-onset cases"

Notably, the study of Srivastava *et al.*[3] provides good examples of how CES can affect clinical practice: potential applications include reproductive planning; earlier diagnosis in other family members; altered prognosis; further disease monitoring or work-up for expected complications; medication changes; and participation in clinical therapeutic trials. These benefits are most relevant to paediatric patients.

The study of Srivastava *et al.*[3] also highlights one of the limitations of CES. As no standard criteria are available to judge variants obtained through CES, each laboratory has its own parameters and, potentially, their own definition of a 'pathogenic variant'. Other technical limitations of CES include the fact that some exons are not fully covered, and CES accuracy varies depending on protocols and kits used or data throughput. After sequencing, variant filtering is required to separate the candidates from the huge numbers of variants obtained through CES. Typically, each laboratory uses its own bioinformatics pipeline to identify candidate variants. Different variants could, therefore, be identified from the same NGS raw data using different pipelines.

As mentioned above, variant filtration and interpretation is a challenging issue. Consensus criteria for evaluating NGS data for clinical use are urgently required. Assessment of the clinical validity of a reported result—that is, whether the variant is clinically compatible, unrelated or atypical (but expanding the phenotypic spectrum)—is also of extreme importance. The ClinVar archive[10] is being developed through international efforts to define clear and definite phenotype–genotype relationships, and might eventually aid interpretation of CES data. Currently, locus-specific databases provide a useful resource for evaluation of variants.

The ethical issues associated with incidental findings, which occur in approximately 1–3% of patients screened with CES, must be considered.[1] The American College of Medical Genetics and Genomics recommends that laboratories screen, and report to the clinician, mutations in a minimum set of 56 genes related to 24 disorders.[1] Genetic counselling before and after screening is particularly important regarding such findings.

The cost of NGS might eventually fall below the costs of clinical diagnosis, leading to 'genotyping first' followed by clinical examination of a patient. If neurology practice does move toward this 'reverse phenotyping framework', as Srivastava *et al.*[3] imply, clinical diagnosis to confirm the pathogenicity of the mutation would become more important, but is expected to be rather challenging, as it will require more neurologists with expertise in NGS.

*Department of Human Genetics, Yokohama City University Graduate School of Medicine, 3–9 Fukuura, Kanazawa-ku, Yokohama 236–0004, Japan (**S.M., N.M.**).*
Correspondence to: N.M.
naomat@yokohama-cu.ac.jp

Acknowledgements
The authors' work is supported by grants from the Ministry of Health, Labour and Welfare of Japan, Grants-in-Aid for Scientific Research (A and C) from the Japan Society for the Promotion of Science, the Takeda Science Foundation, the fund for Creation of Innovation Centres for Advanced Interdisciplinary Research Areas Program in the Project for Developing Innovation Systems from the Japan Science and Technology Agency, the Strategic Research Program for Brain Sciences, and a Grant-in-Aid for Scientific Research on Innovative Areas (Transcription Cycle) from the Ministry of Education, Culture, Sports, Science and Technology of Japan.

Competing interests
The authors declare no competing interests.

1. Biesecker, L. G. & Green, R. C. Diagnostic clinical genome and exome sequencing. *N. Engl. J. Med.* **370**, 2418–2425 (2014).
2. Fogel, B. L. *et al.* Exome sequencing in the clinical diagnosis of sporadic or familial cerebellar ataxia. *JAMA Neurol.* **71**, 1237–1246 (2014).
3. Srivastava, S. *et al.* Clinical whole exome sequencing in child neurology practice. *Ann. Neurol.* **76**, 473–483 (2014).
4. Majewski, J., Schwartzentruber, J., Lalonde, E., Montpetit, A. & Jabado, N. What can exome sequencing do for you? *J. Med. Genet.* **48**, 580–589 (2011).
5. Ng, S. B. *et al.* Exome sequencing identifies the cause of a mendelian disorder. *Nat. Genet.* **42**, 30–35 (2010).
6. Yang, Y. *et al.* Clinical whole-exome sequencing for the diagnosis of mendelian disorders. *N. Engl. J. Med.* **369**, 1502–1511 (2013).
7. Koboldt, D. C., Steinberg, K. M., Larson, D. E., Wilson, R. K. & Mardis, E. R. The next-generation sequencing revolution and its impact on genomics. *Cell* **155**, 27–38 (2013).
8. de Ligt, J. *et al.* Diagnostic exome sequencing in persons with severe intellectual disability. *N. Engl. J. Med.* **367**, 1921–1929 (2012).
9. Rauch, A. *et al.* Range of genetic mutations associated with severe non-syndromic sporadic intellectual disability: an exome sequencing study. *Lancet* **380**, 1674–1682 (2012).
10. NCBI Resource Coordinators. Database resources of the National Center for Biotechnology Information. *Nucleic Acids Res.* **42**, D7–D17 (2014).

nature COMMUNICATIONS

ARTICLE

Received 8 Oct 2013 | Accepted 30 Apr 2014 | Published 2 Jun 2014

DOI: 10.1038/ncomms5011

De novo SOX11 mutations cause Coffin–Siris syndrome

Yoshinori Tsurusaki[1,*], Eriko Koshimizu[1,*], Hirofumi Ohashi[2], Shubha Phadke[3], Ikuyo Kou[4], Masaaki Shiina[5], Toshifumi Suzuki[1,6], Nobuhiko Okamoto[7], Shintaro Imamura[8], Michiaki Yamashita[8], Satoshi Watanabe[9], Koh-ichiro Yoshiura[9], Hirofumi Kodera[1], Satoko Miyatake[1], Mitsuko Nakashima[1], Hirotomo Saitsu[1], Kazuhiro Ogata[5], Shiro Ikegawa[4], Noriko Miyake[1] & Naomichi Matsumoto[1]

Coffin–Siris syndrome (CSS) is a congenital disorder characterized by growth deficiency, intellectual disability, microcephaly, characteristic facial features and hypoplastic nails of the fifth fingers and/or toes. We previously identified mutations in five genes encoding subunits of the BAF complex, in 55% of CSS patients. Here we perform whole-exome sequencing in additional CSS patients, identifying *de novo SOX11* mutations in two patients with a mild CSS phenotype. *sox11a/b* knockdown in zebrafish causes brain abnormalities, potentially explaining the brain phenotype of CSS. SOX11 is the downstream transcriptional factor of the PAX6–BAF complex, highlighting the importance of the BAF complex and SOX11 transcriptional network in brain development.

[1] Department of Human Genetics, Yokohama City University Graduate School of Medicine, 3-9 Fukuura, Kanazawa-ku, Yokohama 236-0004, Japan. [2] Division of Medical Genetics, Saitama Children's Medical Center, 2100 Magome, Iwatsuki 339-8551, Japan. [3] Department of Medical Genetics, Sanjay Gandhi Postgraduate Institute of Medical Sciences, Raebareli Rd, Lucknow 226014, India. [4] Laboratory for Bone and Joint Diseases, Center for Integrative Medical Sciences, RIKEN, 4-6-1 Shirokanedai, Minato-ku, Tokyo 108-8639, Japan. [5] Department of Biochemistry, Yokohama City University Graduate School of Medicine, 3-9 Fukuura, Kanazawa-ku, Yokohama 236-0004, Japan. [6] Department of Obstetrics and Gynecology, Juntendo University, Hongo 3-1-3, Bunkyo-ku, Tokyo 113-8431, Japan. [7] Department of Medical Genetics, Osaka Medical Center and Research Institute for Maternal and Child Health, 840 Murodo-cho, Izumi 594-1101, Japan. [8] National Research Institute of Fisheries Science, 2-12-4 Fukuura, Kanazawa-ku, Yokohama 236-8648, Japan. [9] Department of Human Genetics, Nagasaki University Graduate School of Biomedical Sciences, 1-12-4 Sakamoto, Nagasaki 852-8523, Japan. * These authors contributed equally to this work. Correspondence and requests for materials should be addressed to N.M. (email: naomat@yokohama-cu.ac.jp).

Coffin–Siris syndrome (CSS; MIM#135900) is a congenital disorder characterized by growth deficiency, intellectual disability, microcephaly, characteristic facial features and hypoplastic nails of the fifth fingers and/or toes (Supplementary Fig. 1). Five subunit genes (*SMARCB1*, *SMARCA4*, *SMARCE1*, *ARID1A* and *ARID1B*) of the BAF complex (also known in yeast as the SWI/SNF complex[1]) are mutated in 55–70% of CSS patients[2–6]. Mutations in *SMARCA2*, another BAF complex gene, were reported in the Nicolaides–Baraitser syndrome, which is similar to, but distinct from CSS[7]. Furthermore, *de novo PHF6* mutations were found in two CSS patients[6], although no direct interaction has been reported between the BAF complex and PHF6, which interacts with the nucleosome remodelling and deacetylation complex[6]. As 30–45% of CSS patients were genetically undiagnosed in three large cohort studies[2–6], further genetic investigation is required to fully address the genetic picture of CSS.

Here we apply whole-exome sequencing (WES) to 92 CSS patients, and identify two *de novo SOX11* mutations in two unrelated patients. *sox11* knockdown experiments in zebrafish result in a smaller head and significant mortality, which were partially rescued by human wild-type *SOX11* messenger RNA (mRNA), but not by mutant mRNA.

Results

WES of CSS patients. We identified two *de novo SOX11* mutations in two unrelated patients, c.347A>G (p.Tyr116Cys) (in patient 1) and c.178T>C (p.Ser60Pro) (in patient 2) (deposited to LOVD, http://www.LOVD.nl/SOX11), among 92 CSS patients (including our previous cohorts[2,3]) analysed by trio-based WES. In the two patients, >10 reads covered 94–92% of coding sequences and only *SOX11* mutations remained as candidate variants in both of them based on the *de novo* model with scores of damaging or disease causing by SIFT, PolyPhen2 and Mutation Taster (Supplementary Table 1). The two heterozygous mutations localize to the high-mobility group (HMG) domain. Neither mutation was registered in the databases examined (1,000 Genomes, Exome Sequencing project (ESP) 6500, and in-house databases containing 575 control exomes) (Supplementary Table 1). We identified a further 22 *SOX11* variants within these three databases, but all of them reside outside the HMG domain and, based on prediction programs, are less likely to be pathogenic (Supplementary Table 1; Supplementary Fig. 2). The amino acids altered in SOX11 are evolutionarily conserved from zebrafish to human (Fig. 1). The mutations do not alter nuclear localization of SOX11 protein (Supplementary Fig. 3). *De novo* mutations were confirmed in the two families by Sanger sequencing along with biological parentage. No mutations in any of the other BAF complex genes, *PHF6*, or other potential candidate genes were found in the two families. Therefore, the two mutations identified are highly likely to be pathogenic. Moreover, *SOX11* was sequenced by WES ($n=23$) or Sanger method ($n=67$) in a further 90 CSS patients, with no mutations found. Fifty-four patients had a mutation in one of the five BAF complex subunit genes (58.7%) (*SMARCA4*, *SMARCB1*, *SMARCE1*, *ARID1A* and *ARID1B* mutations found in 9, 8, 1, 5 and 31 patients, respectively).

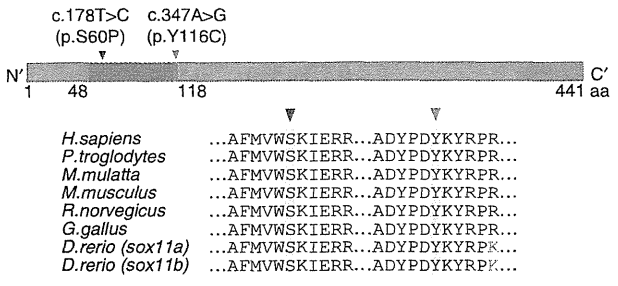

Figure 1 | *SOX11* mutations and functional characterization. *SOX11* mutations in CSS patients. Two missense mutations in the HMG domain (blue box) occur at evolutionarily conserved amino acids.

Clinical features of patients with *SOX11* mutations. The two patients showed dysmorphic facial features, microcephaly, growth deficiency, hypoplastic fifth toe nails and mild intellectual disability[8] (Supplementary Fig. 1; Supplementary Table 2). The observed clinical features in both patients are classified to a mild end of CSS as patient 1 spoke early for CSS and patient 2 has relatively high intelligence quotient. Although the two patients do not look similar in facial appearance (patient 1 has midface hypoplasia, while patient 2 does not; in addition there is an ethnic difference, as patients were either Japanese or Indian), they do share features in common, namely, hypertrichosis, arched eyebrows, low-set ears, auricular back-rotationand full cheeks (Supplementary Fig. 1).

Patient 1 (Japanese) was born at 38 weeks of gestation following an uneventful pregnancy. Her birth weight was 2,340 *g* (−1.9 s.d.), length 45 cm (−2.2 s.d.) and occipitofrontal circumference (OFC) 30.5 cm (−1.8 s.d.). She was hypotonic, had feeding difficulties (especially during the neonatal period) and delayed development. She was able to support her head at 5 months of age, sit at 11 months and walk independently at 1 year 11 months. She started to speak meaningful words at 1 year 7 months. At 3 years, her developmental quotient was estimated using the Kyoto scale of psychological development to be 57. Abdominal echography showed her left kidney was slightly small in size. She has distinctive facial features characterized by midface hypoplasia, short palpebral fissures, hypertelorism, upturned palpebral fissures, long eyelashes, a low nasal root, shortened nose with upturned nostrils, short philtrum, open mouth, full lips and low-set ears. Hypoplastic distal phalanges with nail hypoplasia (especially of the fifth digits) were also noted. Additional findings included hypertrichosis and long eyelashes with abundant hair on the scalp. At 4 years 8 months, she was short with a height of 92.1 cm (−2.9 s.d.) and evaluated for possible growth hormone deficiency with stimulation tests, which showed normal results. At 10 years, she measured 119 cm (−2.8 s.d.), weighed 20.1 kg (−1.8 s.d.) and had an OFC of 47.3 cm (−3.3 s.d.). She attends a special education class for poor performance, but can walk to school by herself (takes approximately half an hour) and is able to communicate verbally, to some extent, with her classmates. Clinical features are summarized in Supplementary Table 2.

Patient 2 (Indian) is a 16-year-old female, and was referred to the genetics outpatient department for evaluation of short stature. She was born at term following a normal pregnancy, but with low birth weight (1.75 kg, −4s.d.). Developmental milestones were attained normally, but her parents always felt that she lagged behind other children. She was a slow learner with poor scholastic performance and an intelligence quotient of 70–80. She attended a normal class, but struggled to pass class examinations every year. She has a proportionately short stature but not a coarse face. Her chin was small and supraorbital ridges hypoplastic with no ptosis. Her nose was long and alae nasi hypoplastic with overhanging columella. Her hair was thick and rough with some thinning on her scalp. She had increased hair on her back. Her fourth and fifth toes were short and all her finger nails were hypoplastic with thin and tapered fingers. Her fourth and fifth toes on both feet, and also the third toe on her right foot, were

markedly hypoplastic. Clinodactyly was noted on the third, fourth and fifth toes on her right foot, and the third and fourth toes on her left foot. A skeletal survey did not show any radiographic bone abnormalities. Her bone age was 13–14 years and follicle-stimulating hormone was 1.57 $IU l^{-1}$ (normal range: <5 $IU l^{-1}$). Ultrasonographic examination at 16 years (before menarche), showed a hypoplastic uterus and malrotation of both kidneys. No secondary sexual characteristics were recognized until she had menarche at 17 years. Now at age of 17 years, she is still short with a height of 141 cm (−5 s.d.), weigh 31.3 kg (−3 s.d.) and OFC 50.5 cm (−4.5 s.d.). Clinical features are summarized in Supplementary Table 2.

Structural effects of SOX11 mutations. To determine the impact of the disease-causing mutations on human SOX11 structure and function, we mapped the mutation positions onto the crystal structure of mouse Sox4[9], that is analogous to human SOX11, and calculated free energy changes on the mutations using FoldX software[10,11]. The mutations lie in the highly conserved HMG domain, responsible for sequence-specific DNA binding (Fig. 2a)[9]. Ser60 is located in a helix of the HMG domain (Fig. 2a), therefore the S60P mutation may affect overall folding of the HMG domain and impair DNA binding of SOX11. FoldX calculations supported this prediction and the free energy change on the mutation was high enough to destabilize protein folding (>10 kcal mol^{-1}) (Fig. 2b)[12]. Conversely, Tyr116 forms a hydrophobic core with the side chains of DNA-recognition loops (Fig. 2a). The Y116C mutation has low free energy change (<1 kcal mol^{-1}) (Fig. 2b), and is unlikely to significantly affect folding of the HMG domain, but instead may alter conformation of the DNA-recognition loop, which is important for DNA binding.

***SOX11* mutations affect downstream transcription.** Both mutations are located within the HMG domain, which is required for *SOX11* transcriptional regulation of *GDF5* (ref. 13). Luciferase assays using the *GDF5* promoter in HeLa and ATDC5 cells, showed both mutant proteins had decreased transcriptional activities compared with wild type (WT) (Fig. 3).

SOX11 expression. *SOX11* transcription levels were examined using multiple human complementary DNA (cDNA) panels. *SOX11* was exclusively expressed in brain (foetus and adult) and heart (adult) tissues, supporting a role for *SOX11* mutations in the brain features of CSS observed in the two patients (Supplementary Fig. 4; Supplementary Table 2).

In mice, targeted *Sox11* disruption with a β-galactosidase marker gene results in 23% birth weight reduction and lethality after the first postnatal week in homozygotes, due to hypoplastic lungs and ventricular septation defects. In addition, skeletal malformations (including phalanges) and abdominal defects are observed[14]. Physical and functional abnormalities in heterozygotes have not been described. However, in heterozygous mice, β-galactosidase expression revealed early ubiquitous expression throughout the embryo with upregulation in the central nervous system (CNS) and limb buds[14].

***sox11* knockdown experiments in zebrafish.** We further investigated *sox11* function in zebrafish. The zebrafish genome contains two orthologs of human *SOX11*, *sox11a* and *sox11b*, which are expressed in all cells until gastrulation and later become restricted to the developing CNS[15,16]. We knocked down zebrafish *sox11a* and *sox11b* (both single-exon genes) using translation-blocking morpholino oligonucleotides (MOs) (*sox11a*-MO, *sox11b*-MO and *sox11a/b*-MO), as previously described[17] (Supplementary Fig. 5a). Off-target effects of morpholino injections were excluded by repeated experiments, co-injecting with *tp53* MO or injecting into $tp53^{zdf1/zdf1}$ mutant fish[18,19]. *sox11a*- and *sox11b*-MO knockdown caused similar phenotypes, including smaller heads and body curvature (Supplementary Fig. 5b). Low-dose *sox11a*- (1.6 ng), *sox11b*- (1.6 ng) and *sox11a/b*- (1.6 ng) MO-injected embryos resulted in

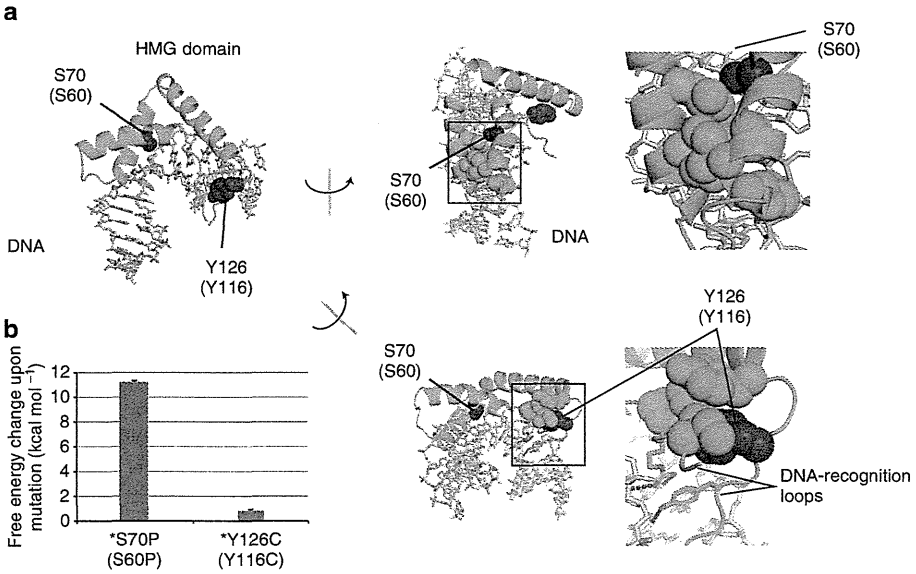

Figure 2 | Structural effects of SOX11 mutations. (**a**) Crystal structure of the mouse Sox4 HMG domain bound to DNA. Helices and loops are shown as green ribbons and threads, respectively. DNA is shown as grey sticks. Amino-acid residues at mutation sites are shown coloured red in the space-filling model. In the middle and right images, some of the amino-acid residues involved in the hydrophobic core surrounding mutation points are shown coloured green in the space-filling model. Amino-acid numbering is indicated for mouse Sox4 with that for human SOX11 in parentheses. Hydrogen bonds are shown as black dotted lines. Molecular structures were drawn using PyMOL (http://www.pymol.org). (**b**) Free energy changes on the indicated mutations calculated by FoldX software.

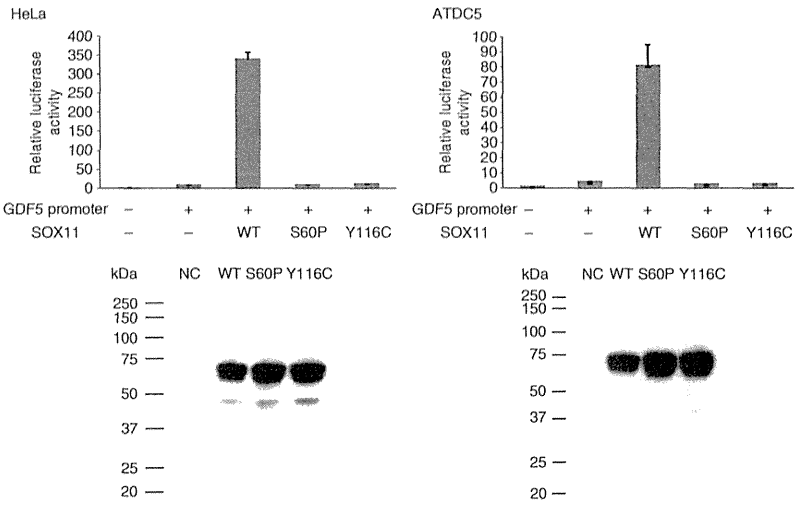

Figure 3 | *SOX11* mutations affecting *GDF5* promoter activity. Luciferase reporter assays measured transcriptional activity of the *GDF5* promoter (−448/+319) (UCSC genome browser hg19: chr20: 34025709-34026457) in HeLa (left) and ATDC5 (right) cells. HeLa or ATDC5 cells were co-transfected with WT or mutant (S60P and Y116C) SOX11 expression vector and reporter constructs containing either GDF5 promoter or empty vector (pGL3-basic). Relative luciferase activities compared with empty vector are presented as mean ± s.d. for two independent experiments, with each experiment performed in triplicate (upper). Immunoblot analysis of transfected HeLa and ATDC5 cell extracts showing wild-type (WT) or mutant (S60P and Y116C) SOX11 proteins (lower). Compared with WT, both SOX11 mutants reduced *GDF5* transcriptional activities in HeLa and ATDC5 cells.

significant mortality (*sox11a*-MO, ~49.3%; *sox11b*-MO, ~19.3%; *sox11a/b*-MO, ~53.0%), compared with control-MO embryos (~7.3%) (Fig. 4a). Co-injection of WT human *SOX11* mRNA (h*SOX11*-WT mRNA) with *sox11a/b*-MO improved morphant survival at 48 h post fertilization (hpf) (25.5% lethality versus 49.3% lethality with *sox11a/b*-MO alone) ($P<0.01$) (Fig. 4a; Supplementary Fig. 5c). The affected phenotype of *sox11a/b* double morphants was partially rescued by h*SOX11*-WT mRNA overexpression (4.5% normal for *sox11a/b*-MO alone versus 36.5% for co-injection with h*SOX11*-WT mRNA and *sox11a/b*-MO, $P<0.01$) (Fig. 4a). In contrast, co-injection of either mutant h*SOX11* mRNA (h*SOX11*-S60P and -Y116C mRNA) with *sox11a/b*-MO showed no significant rescue effects on lethal and affected phenotypes (Fig. 4a). There were significantly more normal phenotypes following h*SOX11*-WT mRNA and *sox11a/b*-MO co-injection, than with h*SOX11*-mutant mRNA co-injections ($P<0.05$). Head sizes in randomly selected embryos ($n\geq10$) of *sox11a* and *sox11a/b* morphants at 48 hpf were significantly decreased ($P<0.05$ in both), but not significantly changed in *sox11b* morphant. Overexpression of h*SOX11*-WT mRNA restores *sox11a/b* double-morphant head size (in randomly selected embryos, $n\geq10$), suggesting specific *sox11* suppression by morpholino injection (Fig. 4b). Although the head size of h*SOX11*-mutant mRNA and *sox11a/b*-MO-injected embryos was slightly decreased, no significant difference was recognized between overexpression of h*SOX11*-WT or h*SOX11*-mutant mRNA and *sox11a/b*-MO co-injection (Fig. 4b).Staining with acridine orange and terminal deoxynucleotidyl TdT-mediated dUTP nick end labelling (TUNEL), found significant apoptotic increases exclusively in microcephalic embryos (Fig. 4c; Supplementary Fig. 6). Brain cell death was prevented by co-injection with h*SOX11*-WT mRNA, but not by mutant h*SOX11* mRNAs (Fig. 4c). We also used HuC/D (a marker for early postmitotic and mature neurons) and acetylated tubulin (an axonal marker) immunostaining at 48 hpf to analyse neuronal cells in more detail (Supplementary Fig. 7). Decreased HuC/D-positive neurons, especially in the telencephalon and diencephalon, were observed in *sox11* morphants (Supplementary Fig. 7a). The phenotype in *sox11a/b*-MO-injected embryos was efficiently rescued by h*SOX11*-WT mRNA (Supplementary Fig. 7a). Reduction of HuC/D-positive neurons was unaltered by mutant h*SOX11* mRNA overexpression and *sox11a/b*-MO injection (Supplementary Fig. 7a). Anti-acetylated tubulin staining also showed severely reduced axonal numbers in the forebrain, midbrain and hindbrain of *sox11* morphants, compared with control-MO-injected embryos (Supplementary Fig. 7b). *sox11a/b* morphants showed phenotypic rescue when co-injected with h*SOX11*-WT mRNA, compared with mutant h*SOX11* mRNAs (Supplementary Fig. 7b).

Discussion

We have identified *SOX11* mutations in CSS. This is the first report of human mutations in *SOXC* (*SOX4*, *SOX11* and *SOX12*)[20]. *SOX11*/*sox11* is required for neurogenesis, and loss of function in early embryos is sufficient to impair normal CNS development. Haploinsufficiency of other *SOX* genes (*SOX2*, *SOX9* and *SOX10*) is known to cause human diseases[21–23]. It is interesting that mutations of *SOX11* and other BAF subunit genes are mutually exclusive in CSS.

Sox11 was recently shown to form a transcriptional cross-regulatory network downstream of the Pax6–BAF complex. The network drives neurogenesis and converts postnatal glia into neurons[24]. Brg1 (Smarca4) binds to the *Sox11* promoter, and interaction with Pax6 is sufficient to induce Sox11 expression in neurosphere-derived cells in a Brg1-dependent manner[24]. Therefore, the Pax6–BAF complex activates a cross-regulatory transcriptional network, maintaining high expression of genes involved in neuronal differentiation and execution of cell lineage decisions[24]. *SOX11* mutations appear to be a rare cause of CSS as only 2 out of 92 patients (2.2%) showed *SOX11* abnormality and to be limited to the mild end of CSS phenotype. Abnormality of the upstream BAF complex tends to show a more severe phenotype compared with that of a downstream *SOX11* mutation, which may indicate rather specific effects of *SOX11* mutations on the CSS phenotype.

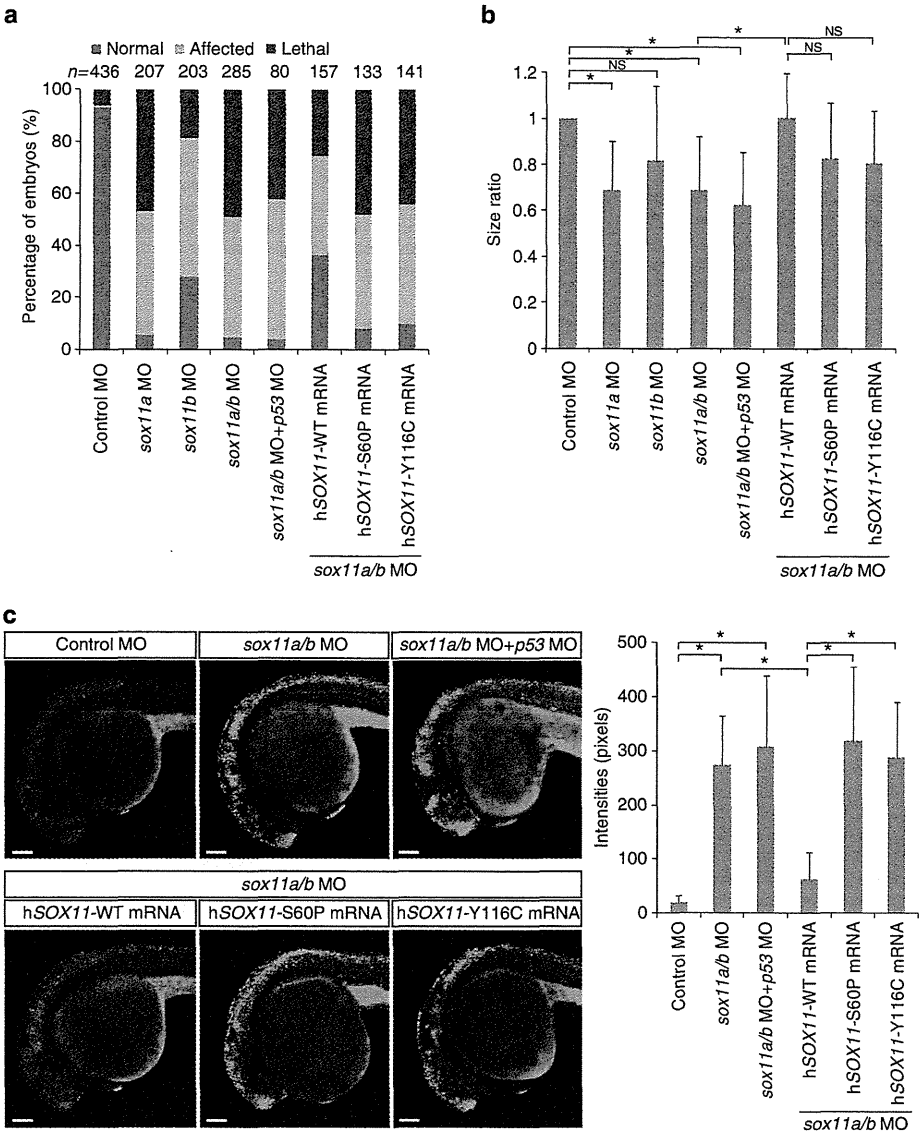

Figure 4 | *sox11a/b* knockdown experiments in zebrafish. (**a**) Embryos were injected with *sox11*-MO alone or with *sox11*- and *tp53*-MO or with *sox11*-MO and *in vitro* transcribed human *SOX11* (h*SOX11*) mRNA (WT, wild type; S60P, p.Ser60Pro; Y116C, p.Tyr116Cys). Injected embryos were categorized as normal, affected and lethal at 48 hpf. The lethal and affected phenotype in *sox11a/b*-MO-injected embryos was partially rescued by WT h*SOX11* mRNA overexpression. All experiments were performed more than twice and evaluated statistically with a Student's *t*-test. (**b**) Head size ratios of embryos with control-, *sox11a*-, *sox11b*- or *sox11a/b*-MO alone, or with *sox11a/b*- and *tp53*-MO or *sox11a/b*-MO and h*SOX11* mRNA (WT or mutant) at 48 hpf ($n \geq 10$) (average of control-MO as 1). Dorsal views of midbrain width were measured. Data are represented as mean ± s.d. $^*P < 0.05$ by Student's *t*-test. NS, not significant. (**c**) Brain cell death in MO-injected embryos at 30 hpf using acridine orange staining (lateral view). *sox11* morphants show increased cell death in the CNS. Scale bar, 100 μm. Quantification of acridine orange intensities in morphants are shown graphically (right, $n \geq 10$). Data are represented as mean ± s.d. $^*P < 0.001$ by Student's *t*-test.

In conclusion, mutations in both BAF complex genes and *SOX11* result in the same phenotype (CSS), providing strong support for the BAF complex and SOX11 function in a common pathway, and play an important role in human brain development.

Methods

Subjects and clinical data. Patients were seen by their attending clinical geneticists. DNA samples were isolated from peripheral blood leukocytes using standard methods. Informed consent was obtained from the parents of the patients for experimental protocols and displaying participants' facial appearances in publications. This study was approved by the institutional review board of Yokohama City University School of Medicine. A total of 92 patients were analysed, including 71 patients from a previous cohort and 21 new patients.

WES. Trio-based WES was performed in two families. Briefly, 3 μg of genomic DNA was sheared using the Covaris 2S system (Covaris, Woburn, MA) and partitioned using SureSelect Human All Exon V4 or V4 + UTRs (Agilent Technology, Santa Clara, CA), according to the manufacturer's instructions. Exon-enriched DNA libraries were sequenced using HiSeq2000 (Illumina, San Diego, CA) with 101-bp paired-end reads and 7-bp index reads. Four samples (2.5 pM each, with different indexes) were run in one lane. Image analysis and base calling were performed using HiSeq Control Software/Real-Time Analysis and CASAVA1.8.2 (Illumina). Mapping to human genome hg19 was performed using Novoalign (http://www.novocraft.com/main/page.php?s=novoalign). Aligned reads were

processed by Picard (http://picard.sourceforge.net) to remove PCR duplicates. Variants were called using the Genome Analysis Toolkit 1.5–21 (GATK v3) with best practice variant detection (http://gatkforums.broadinstitute.org/discussion/15/best-practice-variant-detection-with-the-gatk-v1-x-retired), and annotated by Annovar (23 February 2012) (http://www.openbioinformatics.org/annovar/). Common variants registered in dbSNP137 (MAF≥0.01) (http://genome.ucsc.edu/cgi-bin/hgTrackUi?hgsid=281702941&c=chr1&g=snp137Flagged) were removed.

Prioritization of variants. From all the variants within exons and ±2 bp of intronic regions from exon–intron boundaries, those registered in either dbSNP137, 1,000 Genomes (http://www.1000genomes.org/), ESP 6500 (http://evs.gs.washington.edu/EVS/) or our in-house (exome data from 408 individuals) databases, and those located within segmental duplications, were removed and we focused on heterozygous non-synonymous and splice site variants, which were subsequently confirmed by Sanger sequencing. *SOX11* mutations in LOVD, http://www.LOVD.nl/SOX11.

Structural modelling and free energy calculations. The crystal structure of the mouse Sox4 HMG domain bound to DNA (Protein Data Bank code 3U2B) was selected by SWISS-MODEL server 5 (ref. 25) as the structure most resembling human SOX11. To examine the missense mutations, mutational free energy changes were calculated using FoldX software (version 3.0)[10,11]. Calculations were repeated three times, and resultant data presented as average values with s.d.

***SOX11* expression analysis in human tissues.** TaqMan quantitative real-time PCR was performed using cDNAs from adult (Human MTC Panel I, #636742, Clontech Laboratories, Mountain View, CA) and foetus (Human Fetal MTC Panel, #636747, Clontech Laboratories). Pre-designed TaqMan probes for human *SOX11* (Hs00167060_m1, Life Technologies Co., Carlsbad, CA) and human beta-actin (ACTB, 4326315E, Life Technologies Co.) were used. PCR was performed on a Rotor-Gene Q (QIAGEN, Valencia, CA) and expression levels normalized to *ACTB*, an internal standard gene, according to the $2^{-\Delta\Delta Ct}$ method. Kidney expression was used as the standard (1×).

Expression vectors. The *SOX11* open-reading frame clone was purchased from Promega (Tokyo, Japan) and *SOX11* mutants (c.178T>C; p.Ser60Pro and c.347A>G; p.Tyr116Cys) generated by site-directed mutagenesis with the KOD-Plus-Mutagenesis Kit (TOYOBO, Osaka, Japan). WT and mutant *SOX11* cDNAs were PCR amplified and cloned into the pEF6/V5-His B mammalian expression vector (Life Technologies) using the In-Fusion PCR Cloning Kit (Clontech Laboratories), and also into the p3xFLAG-CMV-14 mammalian expression vector (Sigma, St Louis, MO). The *GDF5* promoter 5′-flanking sequence (−448/+319) was PCR amplified and cloned into the pGL3-basic vector (Promega). All constructs were verified by Sanger sequencing. Human *SOX11* cDNA can be obtained from GenBank/EMBL/DDBJ nucleotide core database under the accession code AB028641.1.

Immunostaining. Mouse neuroblastoma 2A (Neuro-2A) cells were cultured in Dulbecco's modified Eagle's medium (DMEM)–high glucose GlutaMAX supplemented with 10% fetal bovine serum (FBS) and penicillin-streptomycin (Life Technologies Co.). Neuro-2A cells were plated into 24-well plates, 24 h before transfection. Each expression construct (200 ng) was transfected into Neuro-2A cells using X-tremeGENE 9 DNA Transfection Reagent (Roche Diagnostics, Indianapolis, IN). Twenty-four hours after transfection, cells were fixed in 4% paraformaldehyde (PFA)/phosphate-buffered saline (PBS) for 15 min at room temperature, and permeabilized in 0.1% Triton X-100/PBS for 5 min at room temperature. C-terminal V5-6xHis-tagged SOX11 proteins were detected using a mouse anti-V5 primary antibody (1:200; Life Technologies Co.) and an Alexa Fluor 546 Goat Anti-Mouse IgG secondary antibody (1:1,000; Life Technologies Co.). Smears were mounted in Vectashield mounting medium with DAPI (Vector Lab., Burlingame, CA). Confocal images were acquired using a Fluoview FV1000-D microscope (Olympus, Tokyo, Japan).

Luciferase assay. HeLa cells were cultured in DMEM-high glucose supplemented with penicillin (50 units ml^{-1}), streptomycin (50 μg ml^{-1}) and 10% FBS. ATDC5 cells were cultured in DMEM/Ham's F-12 (1:1) supplemented with the above antibiotics and 5% FBS. Cells were plated in 24-well plates, 24 h before transfection, and transfections performed using TransIT-LT1 (Takara, Ohtsu, Japan) with pGL3 reporter (500 ng per well), effector (250 ng per well) and pRL-SV40 internal control (6 ng per well) vectors. Twenty-four hours after transfection, cells were harvested and luciferase activities measured using the PicaGene Dual SeaPansy Luminescence Kit (TOYO B-Net, Tokyo, Japan). Production of WT and mutant SOX11 proteins was assessed by immunoblot analysis with monoclonal anti-FLAG M2 HRP antibody (1:3,000; Sigma), following the manufacturer's instructions.

Morpholino and mRNA microinjection. Antisense translation-blocking morpholinos (MOs) for *sox11a*—(5′-CGCTGTTGTCCGTTTGCTGCACCAT-3′), *sox11b*—(5′-CTGTGCTCCGTCTGCTGCACCATGT-3′)[17], *tp53*—(5′-GCGCCATTGCTTTGCAAGAATTG-3′)[18] and standard control—(5′-CCTCTTACCTCAGTTACAATTTATA-3′) MO were obtained from GeneTools (Philomath, OR) and injected (or co-injected) into one- to two-cell-stage embryos at a final concentration of 0.1 or 0.2 mM. In rescue assays, capped human *SOX11* mRNAs transcribed *in vitro* from pEF6/V5-His B constructs were prepared using the mMessage mMachine T7 ULTRA Transcription Kit (Ambion, Carlsbad, CA), following the manufacturer's instructions, and injected into one-cell-stage embryos. For each MO knockdown and rescue experiment, embryos from the same clutch were used as experimental subjects and controls. Approximately 1 μg of capped RNA was injected per embryo. The experiment was authorized by the institutional committee of fish experiments in the National Research Institute of Fisheries Science.

Cell death detection. To detect apoptotic cells in live embryos, embryos at 30 hpf were manually dechorionated and incubated in acridine orange (2 μg ml^{-1} in egg water) at 28 °C for 1 h. After washing with egg water six times for 10 min each, embryos were anaesthetized with tricaine, mounted in 2% methylcellulose and examined by confocal microscopy. Apoptotic cells were also examined by the TUNEL assay, as previously described[26]. Embryos at 30 hpf, were fixed overnight in 4% PFA with PBS at 4 °C and stored in 100% methanol at −20 °C. Samples were incubated in 100% acetone at −20 °C for 20 min. Following fixation, the embryos were rinsed three times with PBS containing 0.1% Tween-20. Samples were then permeabilized by treatment with 0.5% Triton X-100 and 0.1% sodium citrate in PBS for 15 min. Embryos were subjected to the TUNEL assay by using the ApopTag Red *in situ* Apoptosis Detection Kit (Merck KGaA Millipore, Darmstadt, Germany) according to the manufacture's instruction.

Detection and quantitation of visible and fluorescent images. All animals were photographed under the same conditions using a LSM510 confocal microscope (Carl Zeiss, Jena, Germany). In each animal, acridine orange-positive cells were quantitated using a selection tool in Adobe Photoshop, for a colour range chosen by green colour selection of regions showing visually positive acridine orange staining. For analysis of embryos, defined head regions were selected in each embryo. Following pixel selection, a fuzziness setting of 0 was used, and chosen pixel numbers calculated using the image histogram calculation.

Whole-mount immunohistochemistry. For HuC/D staining, embryos at 48 hpf were fixed in 4% PFA overnight at 4 °C and dehydrated in methanol at −20 °C. For acetylated tubulin staining, embryos at 48 hpf were fixed in Dent's fixative (80% methanol and 20% dimethyl sulphoxide) overnight at 4 °C. Embryos were permeabilized with proteinase K followed by postfixation with 4% PFA and washed with PBSTX (PBS containing 0.5% Triton X-100). After treating with 4% normal goat serum (NGS) in PBSTX for 2 h at room temperature, embryos were incubated with mouse anti-HuC/D (1:500, A21271, Life Technologies Co.) or mouse anti-acetylated tubulin (1:1,000, T7451, Sigma) antibodies in 4% NGS/PBSTX overnight at 4 °C. Embryos were washed five times with PBSTX for 10 min each and incubated with goat anti-mouse fluorescein isothiocyanate secondary antibody diluted in 2% NGS/PBSTX for 2 h at room temperature. After washing five times for 10 min each, embryos were mounted in 2% methylcellulose and examined using a Fluoview FV1000-D confocal microscope (Olympus).

References

1. Ronan, J. L., Wu, W. & Crabtree, G. R. From neural development to cognition: unexpected roles for chromatin. *Nat. Rev. Genet.* **14,** 347–359 (2013).
2. Tsurusaki, Y. *et al.* Mutations affecting components of the SWI/SNF complex cause Coffin-Siris syndrome. *Nat. Genet.* **44,** 376–378 (2012).
3. Tsurusaki, Y. *et al.* Coffin-Siris syndrome is a SWI/SNF complex disorder. *Clin. Genet.* **85,** 548–554 (2014).
4. Santen, G. W. E. *et al.* Mutations in SWI/SNF chromatin remodeling complex gene ARID1B cause Coffin-Siris syndrome. *Nat. Genet.* **44,** 379–380 (2012).
5. Santen, G. W. E. *et al.* Coffin-Siris syndrome and the BAF complex: genotype-phenotype study in 63 patients. *Hum. Mutat.* **34,** 1519–1528 (2013).
6. Wieczorek, D. *et al.* A comprehensive molecular study on Coffin-Siris and Nicolaides-Baraitser syndromes identifies a broad molecular and clinical spectrum converging on altered chromatin remodeling. *Hum. Mol. Genet.* **22,** 5121–5135 (2013).
7. Van Houdt, J. K. *et al.* Heterozygous missense mutations in SMARCA2 cause Nicolaides-Baraitser syndrome. *Nat. Genet.* **44,** 445–449 (2012).
8. Kosho, T. *et al.* Clinical correlations of mutations affecting six components of the SWI/SNF complex: detailed description of 21 patients and a review of the literature. *Am. J. Med. Genet. A* **161,** 1221–1237 (2013).
9. Jauch, R., Ng, C. K., Narasimhan, K. & Kolatkar, P. R. The crystal structure of the Sox4 HMG domain-DNA complex suggests a mechanism for positional interdependence in DNA recognition. *Biochem. J.* **443,** 39–47 (2012).
10. Guerois, R., Nielsen, J. E. & Serrano, L. Predicting changes in the stability of proteins and protein complexes: a study of more than 1000 mutations. *J. Mol. Biol.* **320,** 369–387 (2002).

11. Schymkowitz, J. *et al.* The FoldX web server: an online force field. *Nucleic Acids Res.* **33,** W382–W388 (2005).
12. Khan, S. & Vihinen, M. Performance of protein stability predictors. *Hum. Mutat.* **31,** 675–684 (2010).
13. Kan, A. *et al.* SOX11 contributes to the regulation of GDF5 in joint maintenance. *BMC Dev. Biol.* **13,** 4 (2013).
14. Sock, E. *et al.* Gene targeting reveals a widespread role for the high-mobility-group transcription factor Sox11 in tissue remodeling. *Mol. Cell. Biol.* **24,** 6635–6644 (2004).
15. Rimini, R. *et al.* Expression patterns of zebrafish sox11A, sox11B and sox21. *Mech. Dev.* **89,** 167–171 (1999).
16. de Martino, S. *et al.* Expression of sox11 gene duplicates in zebrafish suggests the reciprocal loss of ancestral gene expression patterns in development. *Dev. Dyn.* **217,** 279–292 (2000).
17. Gadi, J. *et al.* The transcription factor protein sox11 enhances early osteoblast differentiation by facilitating proliferation and the survival of mesenchymal and osteoblast progenitors. *J. Biol. Chem.* **288,** 25400–25413 (2013).
18. Robu, M. E. *et al.* p53 activation by knockdown technologies. *PLoS Genet.* **3,** e78 (2007).
19. Berghmans, S. *et al.* tp53 mutant zebrafish develop malignant peripheral nerve sheath tumors. *Proc. Natl Acad. Sci. USA* **102,** 407–412 (2005).
20. Sarkar, A. & Hochedlinger, K. The sox family of transcription factors: versatile regulators of stem and progenitor cell fate. *Cell Stem Cell* **12,** 15–30 (2013).
21. Fantes, J. *et al.* Mutations in SOX2 cause anophthalmia. *Nat. Genet.* **33,** 461–463 (2003).
22. Pingault, V. *et al.* SOX10 mutations in patients with Waardenburg-Hirschsprung disease. *Nat. Genet.* **18,** 171–173 (1998).
23. Wagner, T. *et al.* Autosomal sex reversal and campomelic dysplasia are caused by mutations in and around the SRY-related gene SOX9. *Cell* **79,** 1111–1120 (1994).
24. Ninkovic, J. *et al.* The BAF complex interacts with Pax6 in adult neural progenitors to establish a neurogenic cross-regulatory transcriptional network. *Cell Stem Cell* **13,** 403–418 (2013).
25. Kiefer, F., Arnold, K., Kunzli, M., Bordoli, L. & Schwede, T. The SWISS-MODEL Repository and associated resources. *Nucleic Acids Res.* **37,** D387–D392 (2009).
26. Koshimizu, E. *et al.* Embryonic senescence and laminopathies in a progeroid zebrafish model. *PLoS ONE* **6,** e17688 (2011).

Acknowledgements

We thank the individuals and their families for participation in this study. We also thank Nobuko Watanabe for her technical assistance. This work was supported by the Ministry of Health, Labour and Welfare of Japan; the Japan Society for the Promotion of Science (a Grant-in-Aid for Scientific Research (B), and a Grant-in-Aid for Scientific Research (A)); the Takeda Science Foundation; the fund for Creation of Innovation Centers for Advanced Interdisciplinary Research Areas Program in the Project for Developing Innovation Systems; the Strategic Research Program for Brain Sciences; and a Grant-in-Aid for Scientific Research on Innovative Areas (Transcription Cycle) from the Ministry of Education, Culture, Sports, Science and Technology of Japan. The Indian Council of Medical Research, New Delhi is also appreciated for funding support for the DNA banking facility.

Author contributions

Y.T. and N.Ma. designed and directed the study. Y.T., E.K. and N.Ma. wrote the manuscript. H.O. and S.P. collected samples and provided subjects' clinical information. N.O. evaluated clinical information. Y.T., T.S., S.M., M.N., H.S., S.W., K.-i.Y. and N.Mi. performed exome and Sanger sequencing. E.K., S.Ima. and M.Y. performed zebrafish experiments. I.K. and S.Ike. performed luciferase assays. M.S. and K.O. performed crystal structural analysis. Y.T. and H.K. analysed protein localization.

Additional information

Accession codes: Exome sequence data for CSS patients have been deposited in the Human Genetic Variation Browser under the accession code HGV0000001 (http://www.genome.med.kyoto-u.ac.jp/SnpDB/repository/HGV0000001.html). Access to this data is controlled by the Yokohama City University Data Access Committee.

Supplementary Information accompanies this paper at http://www.nature.com/naturecommunications

Competing financial interests: The authors declare no competing financial interests.

Reprints and permission information is available online at http://npg.nature.com/reprintsandpermissions/

How to cite this article: Tsurusaki, Y. *et al. De novo SOX11* mutations cause Coffin–Siris syndrome. *Nat. Commun.* 5:4011 doi: 10.1038/ncomms5011 (2014).

Expanding the phenotypic spectrum of *TUBB4A*-associated hypomyelinating leukoencephalopathies

Satoko Miyatake, MD, PhD
Hitoshi Osaka, MD, PhD
Masaaki Shiina, MD, PhD
Masayuki Sasaki, MD, PhD
Jun-ichi Takanashi, MD, PhD
Kazuhiro Haginoya, MD, PhD
Takahito Wada, MD, PhD
Masafumi Morimoto, MD, PhD
Naoki Ando, MD, PhD
Yoji Ikuta, MD
Mitsuko Nakashima, MD, PhD
Yoshinori Tsurusaki, PhD
Noriko Miyake, MD, PhD
Kazuhiro Ogata, MD, PhD
Naomichi Matsumoto, MD, PhD
Hirotomo Saitsu, MD, PhD

Correspondence to Dr. Matsumoto: naomat@yokohama-cu.ac.jp or Dr. Saitsu: hsaitsu@yokohama-cu.ac.jp

Supplemental data at Neurology.org

ABSTRACT

Objective: We performed whole-exome sequencing analysis of patients with genetically unsolved hypomyelinating leukoencephalopathies, identifying 8 patients with *TUBB4A* mutations and allowing the phenotypic spectrum of *TUBB4A* mutations to be investigated.

Methods: Fourteen patients with hypomyelinating leukoencephalopathies, 7 clinically diagnosed with hypomyelination with atrophy of the basal ganglia and cerebellum (H-ABC), and 7 with unclassified hypomyelinating leukoencephalopathy, were analyzed by whole-exome sequencing. The effect of the mutations on microtubule assembly was examined by mapping altered amino acids onto 3-dimensional models of the αβ-tubulin heterodimer.

Results: Six heterozygous missense mutations in *TUBB4A*, 5 of which are novel, were identified in 8 patients (6/7 patients with H-ABC [the remaining patient is an atypical case] and 2/7 patients with unclassified hypomyelinating leukoencephalopathy). In 4 cases with parental samples available, the mutations occurred de novo. Analysis of 3-dimensional models revealed that the p.Glu410Lys mutation, identified in patients with unclassified hypomyelinating leukoencephalopathy, directly impairs motor protein and/or microtubule-associated protein interactions with microtubules, whereas the other mutations affect longitudinal interactions for maintaining αβ-tubulin structure, suggesting different mechanisms in tubulin function impairment. In patients with the p.Glu410Lys mutation, basal ganglia atrophy was unobserved or minimal although extrapyramidal features were detected, suggesting its functional impairment.

Conclusions: *TUBB4A* mutations cause typical H-ABC. Furthermore, *TUBB4A* mutations associate cases of unclassified hypomyelinating leukoencephalopathies with morphologically retained but functionally impaired basal ganglia, suggesting that *TUBB4A*-related hypomyelinating leukoencephalopathies encompass a broader clinical spectrum than previously expected. Extrapyramidal findings may be a key for consideration of *TUBB4A* mutations in hypomyelinating leukoencephalopathies. ***Neurology*® 2014;82:2230-2237**

GLOSSARY

4H = hypomyelination, hypodontia, and hypogonadotropic hypogonadism; **H-ABC** = hypomyelination with atrophy of the basal ganglia and cerebellum; **MAP** = microtubule-associated protein; **MREI** = Met-Arg-Glu-Ile; ***TUBB4A*** = tubulin, beta 4A class IVa.

Leukoencephalopathies are a heterogeneous group of disorders affecting the white matter of the brain. It is estimated that approximately 30% to 40% of patients with leukoencephalopathy remain without a specific diagnosis despite extensive investigations.[1] Brain MRI aids diagnosis because distinct MRI patterns enable easier detection of white matter abnormalities and successful categorization.[1,2] Moreover, recent advances in whole-exome sequencing have improved understanding of these clinically defined/undefined disease entities by identifying genetic causes and their phenotypic spectrum. For example, the majority of cases with hypomyelination,

From the Departments of Human Genetics (S.M., M.N., Y.T., N. Miyake, N. Matsumoto, H.S.) and Biochemistry (M. Shiina, K.O.), Yokohama City University Graduate School of Medicine; Division of Neurology (H.O.), Clinical Research Institute, Kanagawa Children's Medical Center, Yokohama; Department of Pediatrics (H.O.), Jichi Medical School, Tochigi; Department of Child Neurology (M. Sasaki), National Center of Neurology and Psychiatry, Tokyo; Department of Pediatrics (J.-i.T.), Kameda Medical Center, Chiba; Department of Pediatric Neurology (K.H.), Takuto Rehabilitation Center for Children, Sendai; Genetic Counselling and Clinical Research Unit (T.W.), Kyoto University School of Public Health; Department of Pediatrics (M.M.), Graduate School of Medical Science, Kyoto Prefectural University of Medicine; Department of Neonatology and Pediatrics (N.A.), Nagoya City University Graduate School of Medical Sciences; and Department of Neurology (Y.I.), Tokyo Metropolitan Children's Medical Center, Japan.

Go to Neurology.org for full disclosures. Funding information and disclosures deemed relevant by the authors, if any, are provided at the end of the article.

hypodontia, and hypogonadotropic hypogonadism (4H syndrome),[3–5] tremor-ataxia with central hypomyelination leukodystrophy (TACH),[6] leukodystrophy with oligodontia (LO),[7,8] or hypomyelination with cerebellar atrophy and hypoplasia of the corpus callosum (HCAHC),[9] which was described in Japan, share some clinical overlap and have *POLR3A* or *POLR3B* mutations in common.[10–14]

Hypomyelination with atrophy of the basal ganglia and cerebellum (H-ABC)[15,16] is characterized by early-onset motor regression and/or delay followed by extrapyramidal symptoms, distinguishing H-ABC from other hypomyelinating leukoencephalopathies caused by *POLR3A* or *POLR3B* mutations. A recurrent de novo *TUBB4A* mutation was recently reported in 11 patients with H-ABC.[17] Of note, *TUBB4A* mutations also cause autosomal dominant DYT4 dystonia,[18,19] a condition that presents with normal brain MRI findings. This suggests that in addition to H-ABC, *TUBB4A* mutations may be widely related to other hypomyelinating leukoencephalopathies. Herein, we describe 8 patients with *TUBB4A* mutations identified by whole-exome sequencing, clarifying their phenotypic spectrum.

METHODS

Study subjects. Fourteen patients with molecularly undiagnosed hypomyelinating leukoencephalopathy were included in the study. Patients were diagnosed based on clinical symptoms and brain MRI findings. Among the 14 patients, 7 were clinically diagnosed with H-ABC and 7 with hypomyelinating leukoencephalopathy that did not meet the criteria for H-ABC, 4H syndrome, or Pelizaeus-Merzbacher disease. Patients with *POLR3A* or *POLR3B* mutations were excluded from this cohort. When available, parental samples were also tested in mutation-positive patients.

Standard protocol approvals, registrations, and patient consents. Experimental protocols were approved by the Committee for Ethical Issues at Yokohama City University School of Medicine. Written informed consent was obtained from all patients or their parents.

Mutation analysis. We performed whole-exome sequencing in 14 patients. Genomic DNA was captured using the SureSelect^{XT} Human All Exon 50 Mb (v3) or 51 Mb (v4) Kit (Agilent Technologies, Santa Clara, CA) and sequenced on either the GAIIx platform (Illumina, San Diego, CA) with 108–base pair paired-end reads or HiSeq2000 (Illumina) with 101–base pair paired-end reads. After filtering against dbSNP135 and 91 in-house normal control exomes, rare protein-altering and splice-site variant calls were obtained for each patient. We identified *TUBB4A* mutation calls and confirmed these mutations by Sanger sequencing. In 4 of 8 patients with *TUBB4A* mutations, parental samples were analyzed by Sanger sequencing to determine the mode of inheritance.

Three-dimensional structure modeling. To determine the effect of *TUBB4A* mutations on microtubule assembly, we mapped mutation positions onto the 3-dimensional structure of the αβ-tubulin heterodimer (Protein Data Bank code 1JFF)[20] and examined their interaction with surrounding molecules.

RESULTS

Identification of *TUBB4A* mutations. Whole-exome sequencing identified 6 heterozygous missense mutations in *TUBB4A*, in 6 of 7 patients with H-ABC (85.7%) and 2 of 7 patients with unclassified hypomyelinating leukoencephalopathy (28.6%) (see table 1 and tables e-1 and e-2 on the *Neurology*® Web site at Neurology.org). Two mutations, c.1228G>A (p.Glu410Lys) and c.745G>A (p.Asp249Asn), were identified in 2 unrelated patients. Two hypomyelinating patients with similar clinical features as those previously reported,[9] carried the c.1228G>A mutation. The c.745G>A mutation was a recurrent mutation reported in patients with H-ABC.[17] The other 5 mutations were novel. None of the mutations were registered in the National Heart, Lung, and Blood Institute Exome Sequencing Project (ESP6500), 1000 Genomes, or our 575 in-house control exomes. The c.5G>A (p.Arg2Gln) missense mutation, identified in a patient with H-ABC, alters Arg2 to Gln. Arg2 is located within the highly conserved, amino-terminal β-tubulin tetrapeptide Met-Arg-Glu-Ile (MREI) motif and is involved in autoregulatory mechanisms for β-tubulin stability. Notably, Arg2 is altered to Gly in a large family with DYT4.[18,19] All of the mutations occur within highly conserved residues, from yeast to human, and among human β-tubulins (figure 1). GERP (Genomic Evolutionary Rate Profiling) scores were high for all mutated residues, and Web-based prediction programs identified all mutations as pathogenic (table e-1). In 4 patients with parental samples available, the mutations occurred de novo (table e-1). In 2 patients, only the mother's sample was available and confirmed as mutation-negative.

Three-dimensional structural modeling analysis. Tubulin heterodimers polymerize longitudinally in a head-to-tail manner, forming protofilaments, which then laterally interact with each other to form microtubules (figure 2). Some mutations fall within longitudinal interaction interfaces, whereas others are near interaction regions for motor proteins and microtubule-associated proteins (MAPs).[21,22] Thr178 of β-tubulin is located at a longitudinal interheterodimer interface, in proximity to the guanine nucleotide–binding pocket of β-tubulin (figure 2). This residue is reportedly important for regulation of αβ-tubulin heterodimer polymerization with GTP[23,24]; therefore, the Thr178Arg mutation may affect the polymerization process. Arg2 and Asp249 of β-tubulin are

Table 1 Clinical features of the patients

	Patient 1[9]	Patient 2[9]	Patient 3	Patient 4[26]	Patient 5[27]	Patient 6	Patient 7	Patient 8
Current age, y, sex	23, M	41, M	15, F	12, M	16, M	10, M	4, M	1, F
Mutation	c.1228G>A	c.1228G>A	c.5G>A	c.745G>A	c.1162A>G	c.745G>A	c.533C>G	c.785G>A
Protein alteration	p.Glu410Lys	p.Glu410Lys	p.Arg2Gln	p.Asp249Asn	p.Met388Val	p.Asp249Asn	p.Thr178Arg	p.Arg262His
Initial diagnosis	Unclassified hypomyelinating leukoencephalopathy[a]	Unclassified hypomyelinating leukoencephalopathy[a]	H-ABC	H-ABC	H-ABC	H-ABC	H-ABC	H-ABC
Age at onset, mo	12	12	1.5	18	3	19	6	2
Maximum motor milestone	Unsupported unstable walking	Unsupported unstable walking	No head control	Walking for a few steps	Rolling over	Supported walking	No head control	No head control
Onset of motor deterioration	10 y	20 y	ND	18 mo	3 mo	19 mo	ND	ND
Intellectual disability	Mild	Moderate	Severe	Severe	Severe	Severe	Severe	Moderate
Motor signs								
Ataxia	+	+	ND	+	ND	+	ND	ND
Tremor	+	+	−	−	−	+	−	ND
Spasticity	+	+	+	+	+	+	ND	+
Babinski sign	+	+	−	+	ND	+	−	+
Rigidity	+	+	+	+	+	+	+	−
Choreoathetosis	−	−	+	+	+	−	−	−
Dystonia	+	+	+	+	+	+	−	−
Brain MRI findings								
Hypomyelination	+	+	+	+	+	+	+	+
Atrophy of the basal ganglia	−	±	+	+	+	+	+	+
Atrophy of the cerebellum	+	+	+	+	+	+	+	−
Atrophy of the corpus callosum	+	+	+	+	+	+	+	−

Abbreviations: H-ABC = hypomyelination with atrophy of the basal ganglia and cerebellum; ND = not determined.
Symbols: + = present; − = absent; ± = minimally detected.
[a] Unclassified hypomyelinating leukoencephalopathy: did not meet the criteria for H-ABC, 4H syndrome (hypomyelination, hypodontia, and hypogonadotropic hypogonadism), or Pelizaeus-Merzbacher disease.

located at an intraheterodimer interface (figures 2 and e-1A). These residues stabilize the β-tubulin T7 loop region, which interacts with α-tubulin within a heterodimer (figure e-1A), indicating that the p.Arg2Gln and p.Asp249Asn mutations may affect tubulin heterodimerization. Glu410 is located on the exposed outer surface that mediates interactions with motor proteins and/or MAPs (figures 2 and e-1B).[21,22] This residue is crucial for the kinesin-microtubule interaction, and thus the p.Glu410Lys mutation may directly impair motor protein and/or MAP interactions with microtubules. Arg262 and Met388 are located near the intra- and interheterodimer interfaces, respectively, and both are also near the interaction region for motor proteins and/or MAPs (figures 2 and e-1, B and C). Arg262 is involved in the hydrophobic core with residues from a loop that interacts with the α-tubulin subunit within the heterodimer, and from helix H12, which interacts with motor proteins and/or MAPs (figures 2 and e-1B). Met388 is involved in the hydrophobic core with residues from helix H11, which interacts with the α-tubulin subunit in the neighboring heterodimer, and from helix H12 (figures 2 and e-1C).[25] Thus, the p.Arg262His and the p.Met388Val mutations may destabilize the hydrophobic core and potentially affect the tertiary structure, resulting in impairment of longitudinal intra- and interheterodimer tubulin interactions, respectively, and/or interaction with motor proteins and/or MAPs.

Clinical features. Clinical information on patients with *TUBB4A* mutations is presented in tables 1 and e-2, and brain MRIs are shown in figures 3 and e-2.

The mean age at onset was 9.2 months, although the age at onset was varied. Initial motor development also varied, with some acquiring unsupported but